

Proposal

Direct measurements of ω mass modification in $A(\pi^-, n)\omega$ reaction and $\omega \rightarrow \pi^0\gamma$ decays

February 9, 2009

K. Ozawa¹, K. Utsunomiya, Y. Watanabe, Y. Komatsu,
S. Masumoto, and R.S. Hayano

Physics department, Graduate School of Science, University of Tokyo

Y. Morino

Center for Nuclear Study, Graduate School of Science, University of Tokyo

¹Contact person, e-mail:ozawa@phys.s.u-tokyo.ac.jp

Contents

| | | |
|----------|--|-----------|
| 1 | Introduction | 3 |
| 2 | Physics Goal | 6 |
| 3 | Experimental Apparatus | 8 |
| 3.1 | Missing mass measurement | 8 |
| 3.1.1 | Beam energy and beam line | 8 |
| 3.1.2 | Neutron counter | 9 |
| 3.1.3 | Expected missing mass resolution | 10 |
| 3.1.4 | Neutron Efficiency | 11 |
| 3.2 | Invariant mass measurement | 13 |
| 3.2.1 | Gamma-ray detector | 13 |
| 3.2.2 | Expected mass resolution | 14 |
| 3.2.3 | Final state interaction | 14 |
| 3.3 | Trigger | 15 |
| 3.4 | Yield and Beam time | 16 |
| 3.5 | Background | 17 |
| 3.6 | Calibration | 18 |
| 3.6.1 | Time-Of-Flight neutron counter | 18 |
| 3.6.2 | Electro-Magnetic Calorimeter | 18 |
| 4 | Cost estimation | 19 |
| 5 | Summary | 20 |

1 Introduction

The origin of the mass of hadrons has been drawing strong interest in nuclear and particle physicists. In QCD, mass of hadrons is composed of a sum of the effective mass of valence quarks, known as constituent quark mass, and their interaction term. The effective mass of valence quarks is determined by chiral property of QCD vacuum. This mechanism is understood as a consequence of the dynamical breaking of chiral symmetry. In hot and/or dense matter, this broken symmetry will be restored either partially or completely and, hence, properties of hadrons, such as mass, decay modes and life time, can be modified. Therefore we can study the chiral property of QCD vacuum by measurements of the in-medium decay of vector mesons. Especially, detailed measurements of mass spectra in QCD medium are essential, since mass spectra of vector mesons can be directly connected to anti-quark quark condensates, which is an order parameter of chiral symmetry, in QCD medium [1]. In this proposed experiment, we focus on vector meson mass spectra in nucleus, since relatively large mass modification is theoretically expected even at nuclear density [2].

Two experimental approaches have been to study hadron properties in nucleus. One approach is a missing mass spectroscopy and another approach is a direct measurement of mass spectra via meson decays. At the moment, two kinds of approaches are realized in independent experiments and no experiment has performed simultaneous measurements.

One remarkable result is achieved by GSI-S236 group [3] using a missing mass spectroscopy. They observe deeply bound 1s states of π^- in $^{115,119,123}\text{Sn}$ using the $\text{Sn}(d,^3\text{He})$ pion-transfer reaction. It's result indicates a reduction of the chiral order parameter, $f_\pi^*(\rho)^2/f_\pi^2 \approx 0.64$, at the normal nuclear density, $\rho = \rho_0$.

Important results are also obtained in direct measurements of mass distribution in nucleus. The KEK-PS E325 experiment [4] measured the e^+e^- decays of light vector mesons ($\rho/\omega/\phi$) made by the 12-GeV proton induced reaction in the target nucleus. Their results show 9% decreasing of ρ meson mass. It can be expected that ω meson has the same mass decreasing as ρ , since both mesons have the same quark contents. In fact, results from the KEK experiment show the same mass decreasing for ω meson. However, ω peak is sitting on ρ 's broad peak and the measurement has small sensitivities for ω meson mass modification. Modification of ρ meson is also detected by TAGX-INS (KEK-TANASHI) group in $\pi^+\pi^-$ channel in $\gamma + ^3\text{He}/^{12}\text{C}$ reaction [5]. The mass spectral modification of ω meson was measured by the CBELSA/TAPS experiment in $\pi^0\gamma$ decay channel in γA reactions [6]. Since ρ mesons have a very small branching ratio (6.0×10^{-4}) to $\pi^0\gamma$ decays,

contribution of ρ meson is negligible in this measurement. Their results are shown in 1 and they obtain 14% decreasing of ω mass. However, it is difficult to extract mass spectra in nucleus and some model calculations are needed to evaluate 14% mass decreasing, since the ω meson has a momentum distribution and the statistics is limited. Recently, CLAS at J-Lab reported mass

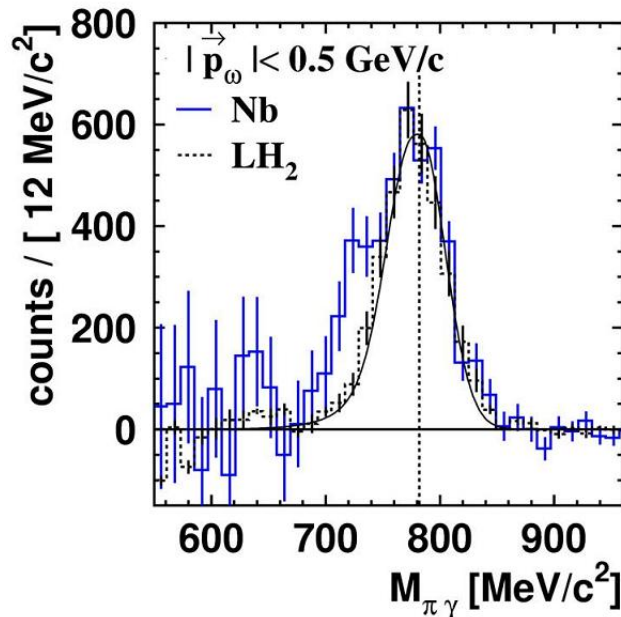


Figure 1: Measured mass spectra of ω meson after background subtraction [6]. Solid line represents Nb target and dotted line represents Liquid hydrogen target.

broadening of ρ meson in γA reactions, though they did not observe mass decreasing [7]. It seems the CLAS result is contradicted with KEK-PS E325 results. However, it should be noted that the reactions used in production of mesons are different and initial conditions of produced mesons should be different. Mass spectrum of vector meson should be different in such different initial condition.

It can be said that the existence of the hadron modification in medium has been established in these experiments. However, the origin of the modification is not clarified yet. The relation between hadron mass modification and the chiral symmetry restoration is not established experimentally. There are two main issues on the current experiments. One problem is that we don't have enough statistics and mass spectra only in limited kinematical region are measured. Another problem is that we don't know the detailed medium

properties and initial conditions of generated meson.

Here we propose measurements of direct ω mass modification in a clear initial condition. Decays of ω meson in nucleus are measured with $\omega \rightarrow \pi^0 \gamma$ mode and initial conditions in produced ω meson are also measured in $A(\pi^-, n)\omega$ reaction. Such exclusive measurement can supply essential information to establish partial restoration of the chiral symmetry in nucleus. Figure 2 shows a schematic view of combined measurements.

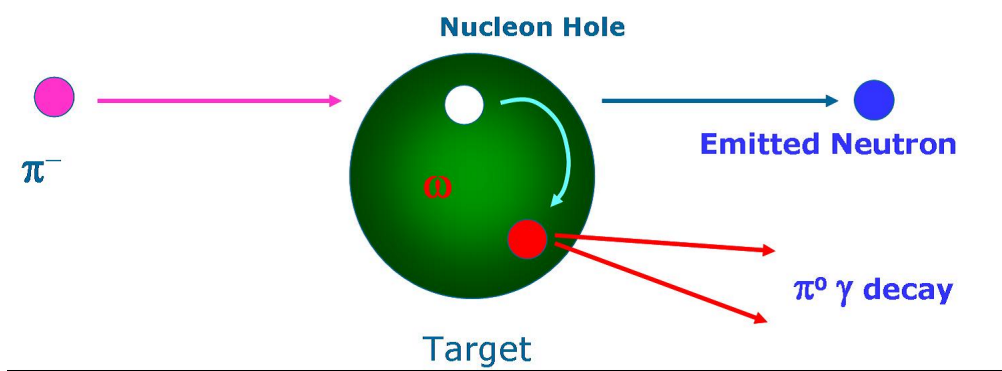


Figure 2: Schematic view of combined measurements

2 Physics Goal

Mass of ω meson at finite density, such as nucleus, has been studied in many theoretical methods. Hatsuda and Lee studied using a QCD sum rule and partial chiral symmetry restoration. They predicted 10~20% decreasing for ρ/ω mass at normal nuclear density [1]. Klingl *et al.* calculated the downward mass-shift and even mass broadening of $\rho/\omega/\phi$ in dense matter[8]. Some models considered couplings to baryon resonances and predicted broadening and slight increasing of ω mass[9, 10]. In addition, ω meson properties have been calculated within varied models ranging from quark models, to phenomenological evaluations, or using effective Lagrangians [11].

One of the current main questions is how we can establish the connection between experimental information and chiral symmetry restoration. In terms of the QCD sum rule, average of the measured spectra of vector meson can be directly interpreted to the square of q-bar q contents of a medium [1]. To obtain measured spectrum in large kinematical space, we will perform another experiment (E16). In addition, we need to know the medium condition which surrounds the generated meson. For this purpose, an exclusive measurement needs to be performed.

In the proposed experiment, measurements of direct ω mass modification in a clear initial condition. Decays of ω meson in nucleus are measured with $\omega \rightarrow \pi^0\gamma$ mode and initial conditions in produced ω meson are also measured in $A(\pi^-, n)\omega$ reaction. Using missing mass information in forward neutron measurements, the generation process of ω meson can be identified. For example, a quasi-free process can be separated and if bounded region is selected in missing mass spectroscopy, we can guarantee that the ω meson really exist in nucleus potential and the measured ω meson mass spectra via the meson decays are for nucleus. In addition, if ω meson is bounded in nucleus and it is observed using the forward neutron measurement, the condition of ω meson in nucleus is established very clearly.

The experiment also aim the direct comparison between experimental results and theoretical prediction in meson mass spectrum in nucleus. Theoretical calculations of meson mass distribution assume that mesons exist at rest in nuclear matter. Thus, previous experiments, such as TAPS and KEK-E325, need some interpretation between experimental results and theoretical predictions to take into account kinematics of generated mesons. In the proposed experiment, measurements of a nuclear ω bound state give kinematical conditions of generated meson. Even if the ω bound state doesn't exist, ω meson is generated in recoil less kinematics and the momentum of generated ω meson is limited within the Fermi motion.

Another issue is a large background in measurements. Evaluation of com-

binatorial background is a major issue in the direct mass measurements via decays. M. Kaskulov *et al.* claims that TPAS results are not robust under shape difference of combinatorial background [14]. Also, huge backgrounds make observation of a broad bound state peak difficult. In the proposed experiment, combined measurements can achieve small background measurement.

In addition, nuclear ω bound states can be measured in $A(\pi^-, n)\omega$ reaction, if the bound state exists. This is the first measurement to see ω bound state in nucleus. Calculations about possible ω bound states have been developed by several groups. W. Weise and his group predict 30 MeV binding energy [12]. H. Nagahiro *et al.* predict 50 MeV binding energy using an optical potential method [13, 14]. Figure 3 shows a prediction of ω bound state from [13].

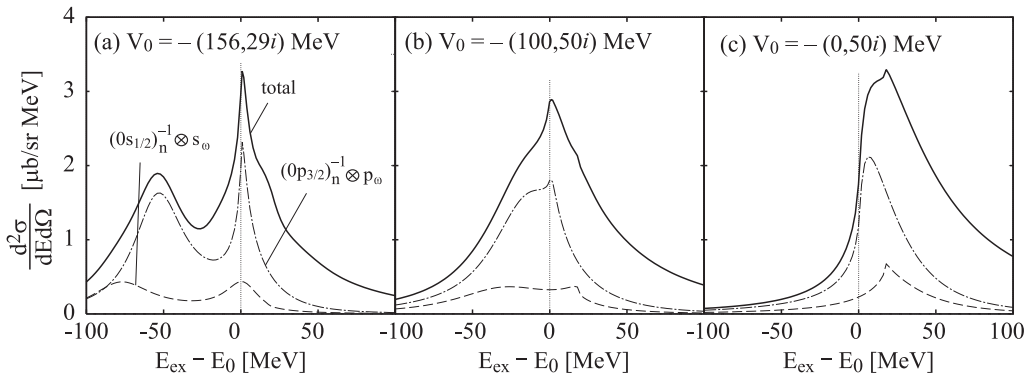


Figure 3: Calculated spectra of $^{12}\text{C}(\pi^+, p)^{11}\text{C} \otimes \omega$ reaction as functions of the excited energy E_{ex} . E_0 is the ω production threshold. The neutron-hole states are indicated as $(nl_j)_n^{-1}$ and the ω states as ℓ_ω [13].

When a binding energy of a ω bound state in nucleus is measured, it can be interpreted to optical potential and gives a phenomenological information about interactions between mesons and nuclei. If mass distribution of bounded ω meson is measured directly via decays, the relation between mass distribution and nuclear-meson interaction is established experimentally. Then, the amount of ω mass shift in direct mass spectrum and ω binding energy can be compared and such comparison gives information about effects beyond the meson nuclei interaction, such as chiral symmetry restoration.

3 Experimental Apparatus

We measured $A(\pi^-, n)\omega$ reaction with forward neutron measurements and decays of generated ω meson with $\omega \rightarrow \pi^0\gamma$ mode and π^0 meson is detected with two γ decays. In the measurements, two detectors are needed. One is neutron detector at the forward region and another is γ detectors for detecting 3 γ 's at target region. Thickness of 6 cm of Carbon-12 is chosen as a target to maximize ω yield.

3.1 Missing mass measurement

We measure incident π meson and forward neutron in $A(\pi^-, n)x$ reaction and calculate missing mass to identify ω meson production. The forward neutron momentum is measured using newly constructed neutron detector and time of flight method.

3.1.1 Beam energy and beam line

Figure 4 shows ω momentum as a function of π^- momentum in $p(\pi^-, n)\omega$ reaction. In this calculation, we assume 9% decreasing of ω meson mass in nucleus, which is measured at KEK. The beam momentum of 1.8 GeV is chosen to have recoil less production of ω meson in nucleus. To obtain the required beam momentum, K1.8 beam line need to be used. The beam intensity of 10^7 of π^- per spill is also required to collect reasonable amount of yield, as described later. Also, emitted neutron should be detected at

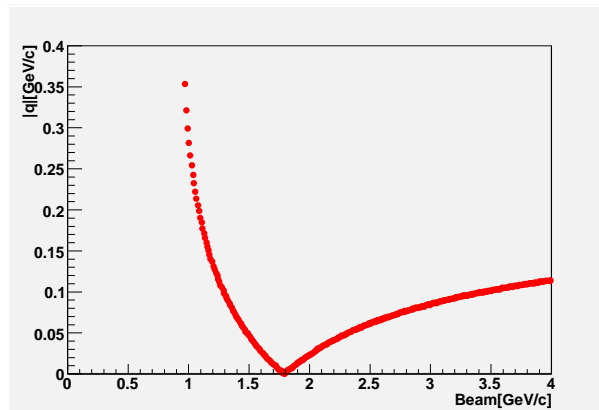


Figure 4: ω momentum as a function of π^- in $p(\pi^-, n)\omega$ reaction.

0 degree to minimize momentum transfer of ω meson. Produced charged

particles and π^- beam are swept by a magnet. The SKS magnet can be used for such sweeping.

Momentum of incident π^- beam is measured by tracking devices at the beam line. The resolution of missing mass measurements is mainly determined by the resolution of forward neutron momentum measurements and the required resolution for π^- momentum is about 1%. As the tracking device, Gas Electron Multiplier (GEM) counters is used, if the beam intensity is too high to operate MWPC.

3.1.2 Neutron counter

Figure 5 shows a schematic view of neutron counter which measure time of flight to identify neutrons and measure neutron momentum. Start timing of the time of flight is measured using incident π^- beam and segmented start counters are used to cope with the high beam intensity.

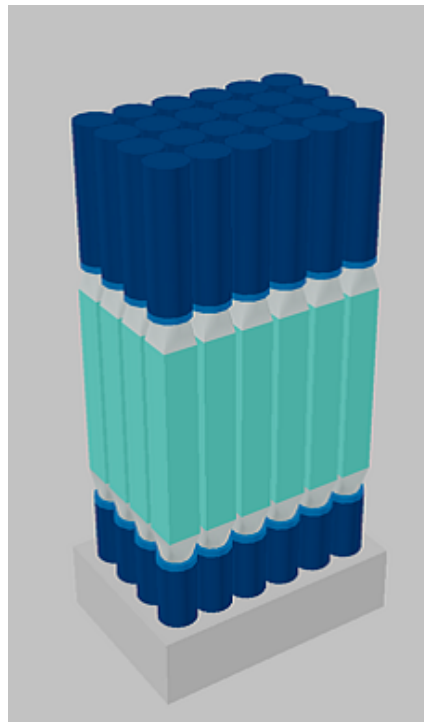


Figure 5: Schematic view of neutron counter

Figure 6 shows a schematic view of the cross section of the neutron counter. The neutron counter consists of two components, such as 1 cm thickness of lead plate as a converter and 5cm thickness of scintillator as a

detector. The counter has 4 layers of the lead plate and scintillator to increase neutron efficiency. The scintillator has 5cm width and 6 scintillators are placed in one layer. The total area of the counter is 30cm by 30 cm and the acceptance ($\delta\theta$) is 1° . According to a theoretical calculation [13] and an experimental result[15], bound state can be generated only for forward neutron and we choose relatively small forward acceptance. In addition, the size of the scintillation counter is limited by the requirement of timing resolution.

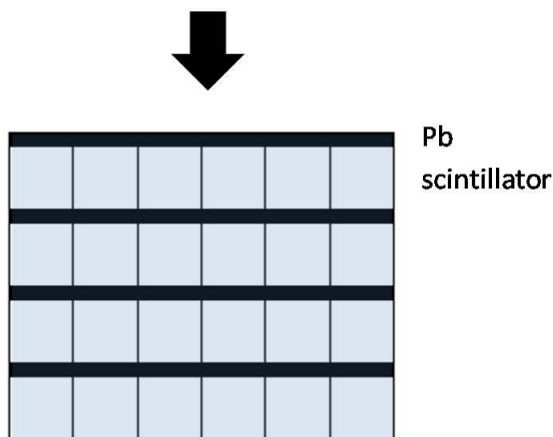


Figure 6: Schematic view of cross section of the neutron counter

3.1.3 Expected missing mass resolution

To achieve enough mass resolution, time resolution should be less than 80 ps. At K1.8 beam line, the maximum flight path is 7m and the mass resolution of $22 \text{ MeV}/c^2$ is achieved.

We perform a simple beam test using electron beam at Fuji test experiment beam line at KEK to choose the best scintillator. We measure time of flight with several combinations of two scintillators with 0 length. Figure 7 shows typical time of flight spectrum at beam test. Results of combination can be broke down to timing resolution of each scintillator. Table 1 shows the timing resolution of each scintillator. Although some scintillators show too good timing resolution and it suggests there is a systematic error, BC404, BC408, and BC420 show enough timing resolution. In fact, in combination of BC420 and BC408, we achieve 55 ps of timing resolution for time of flight measurement.

When 20m flight path is achieved in future experiment at high-momentum beam line, the mass resolution of $9 \text{ MeV}/c^2$ can be achieved and nucleus ω

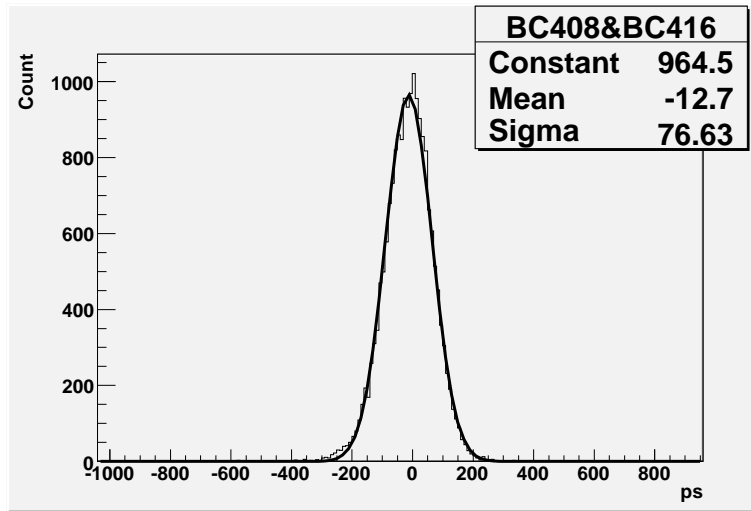


Figure 7: Typical time of flight spectrum at beam test

Table 1: Timing resolution for several scintillators obtained by a beam test

| Scintillator type | BC404 | BC408 | BC412 | BC416 | BC420 |
|-------------------|-------|-------|-------|-------|-------|
| Sigma[ps] | 22.4 | 33.0 | 59.8 | 70.3 | 34.1 |

bound states can be identified easily.

3.1.4 Neutron Efficiency

To evaluate neutron detection efficiency, we perform a Monte Carlo simulation using the FLUKA package [16]. Figure ?? shows the energy distribution of produced particles from lead by neutron. The produced particles emitted from lead to scintillator have enough energy and can be detected with the scintillator.

Particle emission probabilities are summarized in Table 2. When all protons are detected with the scintillator, neutron efficiency of 19% is achieved using 4 layers. It is consistent with a naive calculation using nuclear collision length (114.1 [g/cm²] for lead). In addition, scintillator itself has 2% efficiency with one layer and total 8% efficiency can be expected.

Also, many low energy neutron are produced with hadron interactions and there is a possibility to increase detection efficiency using such neutrons. The response of scintillators for low energy neutrons are checked using neutron

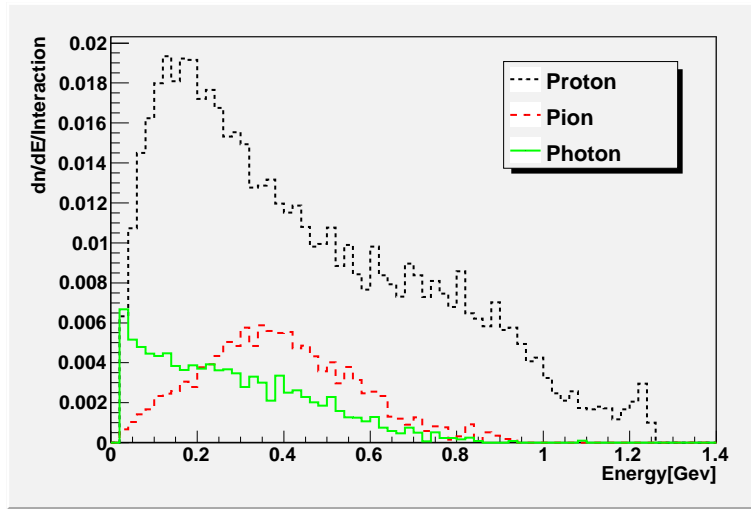


Figure 8: Energy distribution of produced particles from lead by neutron

Table 2: Particle emission probabilities

| | |
|-------------------------|--------|
| Protons per one neutron | 5.1 % |
| Pions per one neutron | 0.91 % |
| Photons per one neutron | 2.0 % |

source (Cf-252). Results are shown in Fig. 9.

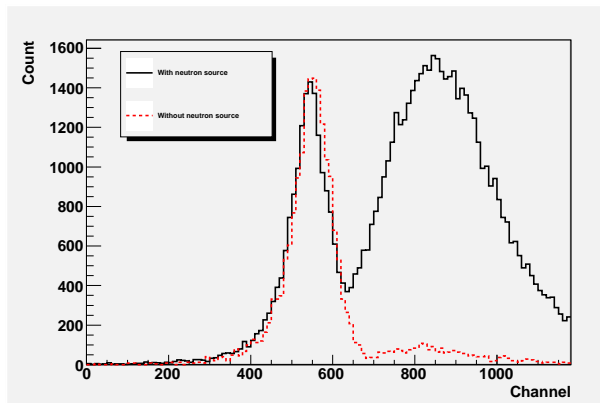


Figure 9: Time of flight measurement for neutron using Cf-252. Dotted and solid lines represent with and without neutron absorber.

3.2 Invariant mass measurement

In this experiment, decays of ω meson are measured using $\omega \rightarrow \pi^0\gamma$ mode and π^0 meson is detected with two γ decays. Thus, total three γ 's need to be detected. The ω meson is generated almost at rest and decayed γ and π^0 goes to back to back. Thus, large acceptance is needed for the γ detection.

3.2.1 Gamma-ray detector

Figure 10 shows a schematic view of the gamma counter which consists of CsI crystal and is used at KEK E246 experiment. The read out of the detector will be upgraded for a new T-violation experiment(E06) at J-PARC. The detector has 12 acceptance holes for requirements of the T-violation experiment. However, it's coverage is still 75 %. These holes cause both decreasing of acceptance and resolution of γ energy measurements. However, it's still enough for the proposed experiment, as described below. The details of the detector are shown in Table 3 and also in [17] and J-PARC E06 proposal. Acceptance of the detector for $\omega \rightarrow \pi^0\gamma$ decays is 58%. Decayed π^0 and γ has back to back configuration, since ω meson is generated almost at rest, and we still have a large acceptance for ω decays. Note: Fermi motion is took into account in this calculation.

The performance of gamma detector as a π^0 detector is evaluated at KEK-PS and summarized in Table 4 [17].

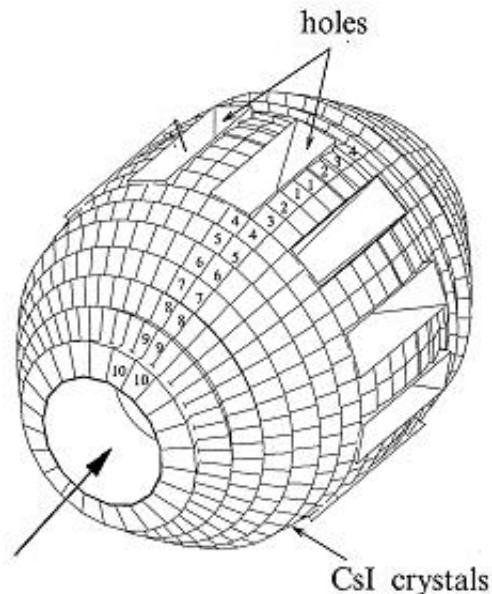


Figure 10: Schematic view of gamma detector [17]

3.2.2 Expected mass resolution

Figure 11 shows invariant mass of ω meson smeared by energy resolution of gamma detector. Effects of the target thickness and the position resolution of gamma ray detection are also considered. Left and right figures are for different energy resolutions. Two cases are considered: 1) $\delta E/E = 1.62\%/\sqrt{E} + 0.8\%$, $\sigma_E/E = 4.3\%$ at 100 MeV and 2.8% at 200 MeV, as shown in Table 4, are assumed and calculated energy dependence of the resolution, 2) $\delta E/E = 3\%/\sqrt{E}$, conservative estimation for the energy resolution. For both cases, two mass peaks can be separated. In the proposed experiment, ω meson generated at rest and ω mesons decayed in free space (right peak) are strongly suppressed and ω meson mass spectra in nucleus can be measured.

3.2.3 Final state interaction

Another issue is the final state interaction of π^0 . It is evaluated for TAPS experiment using a transport model [22]. Figure 12 shows the calculation in [22]. According to this calculation, when π^0 is scattered in nucleus, mass distribution of ω have very large shift in lower side and the effect is negligible in interested mass region, i.e. just below ω mass. However, for 40% of ω mesons, the final state π^0 does rescatter in nucleus.

Table 3: Specification of CsI calorimeter [17]

| | |
|----------------------|---|
| Crystal | CsI(Tl) |
| Segmentation | $\Delta\theta = \Delta\phi = 7.5^\circ$ |
| Number of crystals | 768 |
| Length of a crystal | 25cm($13.5X_0$) |
| Readout | one PIN diode per crystal |
| Total crystal weight | 1700kg |
| Inner diameter | 40cm |
| Outer diameter | 100cm |
| Detector length | 141cm |
| Solid angle coverage | 75% of 4π |

Table 4: Parameters of the CsI π^0 detector [17]

| | |
|--------------------------------|------------------------------------|
| Average light yield | 11000 p.e./MeV |
| Equivalent noise level | 75 keV per module |
| Correlated noise level | 11 keV per module |
| Energy resolution σ_E/E | 4.3% at 100 MeV 2.8% at 200 MeV |
| Spatial resolution (rms) | 7.6 mm at 200 MeV |
| Angular resolution (rms) | 2.2-2.4° |

3.3 Trigger

Trigger is a coincidence of more than 2 γ 's in the calorimeter and one neutron detected at the forward counter. Although the ω decay contain 3 γ 's, it is difficult to separate 2 γ 's from π^0 decays at the trigger level. Then, main background at the trigger is $p(\pi^-, n)\pi^0$ reaction. Figure 13 shows measured total cross section for the reactions $\pi^-p \rightarrow X$. The cross section of the π^0 production at the backward direction is also measured as 0.1 mb/sr (CM frame) [19]. In addition, $p(\pi^-, n)2\pi^0$ also exists and the cross section of the reaction is estimated as 0.06 mb/sr (CM frame), using the total cross section and the angular distribution measured at slightly lower beam momentum [20]. The trigger rate is evaluated using above numbers and it becomes 20 events per spill.

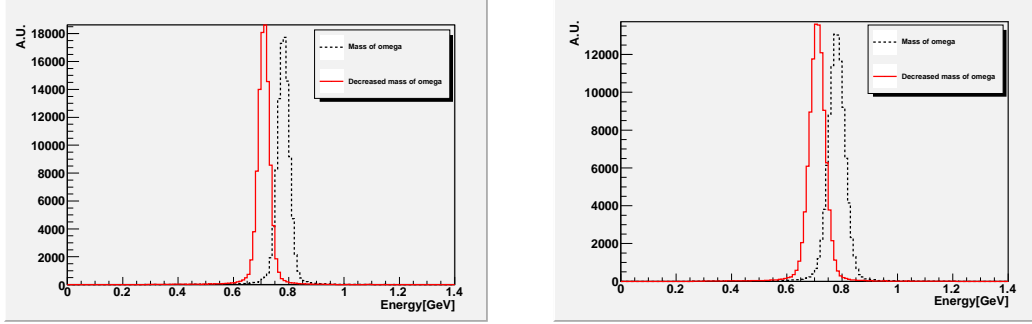


Figure 11: Invariant mass of ω meson smeared by energy resolution of gamma detector. Two lines represent ω mass shift =0(dotted line), 9%(solid line). Mass decreasing of 9% is measured at KEK-E325. Left and Right figures are for different energy resolutions, such as $\delta E/E = 1.62\%/\sqrt{E} + 0.8\%$ and $3\%/\sqrt{E}$.

3.4 Yield and Beam time

Obtained ω yield is estimated with measured cross section in $p(\pi^-, n)\omega$ reaction [21]. Figure 14 shows a summary plot of cross sections of backward ω production as a function of $\cos\theta_\omega$ [18]. The proposed experiment is at $\sqrt{s} = 2.0$ GeV and $\cos\theta_\omega = -1.0$. The production cross section of 0.04 mb/sr (CM frame), which corresponds to 0.17 mb/sr at Lab frame, is used for the estimation. The estimated yield is 470 events per shift and beam time of 100 shifts are required to collect reasonable amount of events. Numbers used in the calculation are summarized in Tab. 5

Table 5: Numbers for yield calculation

| | |
|---|----------------------------------|
| Beam Intensity | 10^7 per spill |
| ω production cross section in π^-p | 0.17 mb/sr in Lab frame |
| Target | Carbon (6 protons, A=12.01) |
| Target thickness | 6 cm (13.59[g/cm ²]) |
| Acceptance of Forward Neutron | 9.57×10^{-4} sr |
| Efficiency of Forward Neutron | 27% |
| Branching ratio of $\omega \rightarrow \pi^0\gamma$ | 8.9% |
| Acceptance of decayed gamma | 58% |
| Radiation loss in Target | 11% |
| Without final state interaction | 60% |
| Spill Duration | 3s |

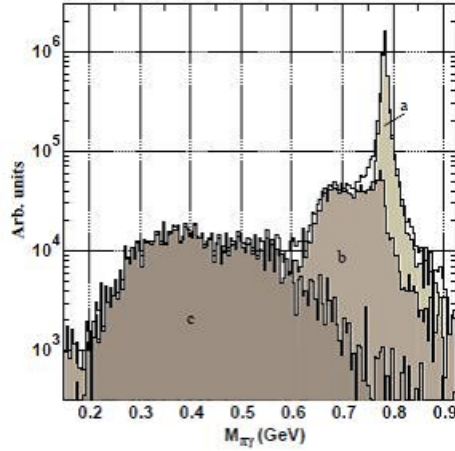


Figure 12: The $\pi^0\gamma$ mass distribution obtained from a Monte Carlo simulation of the process $\gamma + \text{Nb} \rightarrow \pi^0\gamma + X$ at $E_\gamma = 1.2$ GeV. The spectrum is decomposed into different contributions corresponding to the fraction of ω -mesons decaying outside the nucleus (a), the fraction of ω -mesons decaying inside for which the π^0 does not rescatter (b), and the fraction of ω -mesons decaying inside the nucleus for which π^0 rescatters (c).

3.5 Background

The main background in the final plot comes from $p(\pi^-, n)2\pi^0$ reactions. The background in 3 γ 's measurements is 2 π^0 decays and 1 γ missing in the reaction. It's probability is about 25%. When we require that forward neutron has the momentum of 1.74 to 1.86, which corresponds to neutron momentum range of modified ω meson production, the background in ω mass region is suppressed to 0.78 % of the originally produced $2\pi^0$ and expected signal to noise ratio is 30 after subtracting a combinatorial background. The combinatorial background is caused by non-correlated pairs and it can be subtracted using a mixed event method.

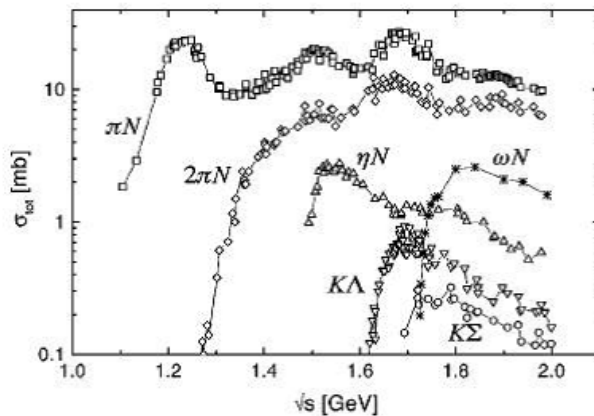


Figure 13: Total cross sections for the reactions $\pi^-p \rightarrow X$ with X as given in the figure [18].

3.6 Calibration

3.6.1 Time-Of-Flight neutron counter

We will use gamma ray for timing calibration of each modules. In addition, we can use forward neutron in $A(\pi^-, n)\pi^0$ reaction.

3.6.2 Electro-Magnetic Calorimeter

We can use decayed gamma rays in $A(\pi^-, n)\pi^0$ reaction. When we reconstruct π^0 , energy calibration of each module can be done. Details of calibration of calorimeter are also discussed in E06 proposal.

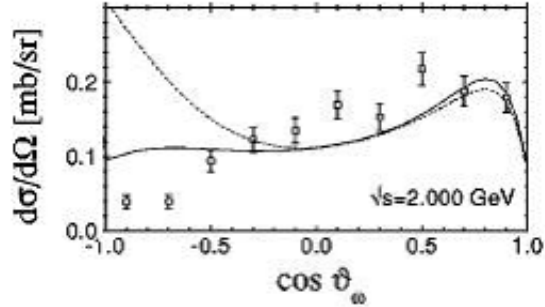


Figure 14: summary plot of differential cross sections of ω production as a function of $\cos\theta_\omega$ [18]. Points represent measurements. Lines represent theoretical calculations, which are not used in this proposal.

4 Cost estimation

A brief cost estimation is shown in Table 6.

Table 6: cost estimation

| Detector | element | description | Budget | cost [M Yen] |
|-----------------|---------------|------------------------|----------------|--------------|
| Beam Line | Tracker | MWPC | Common use | 0 |
| | Start Counter | Segmented scintillator | Common use | 0 |
| Neutron Counter | Frame | | Grant(Kakenhi) | 1 |
| | PMT | 48 x H2431 | Grant(Kakenhi) | 10 |
| | Scintillator | 24 pieces | Grant(Kakenhi) | 2 |
| CsI Carolimeter | | Reuse of E06 | | 0 |
| Total | | | 13 | |

5 Summary

We propose combined measurements of nuclear ω bound state and direct ω mass modification. Nuclear ω bound states are measured in $A(\pi^-, n)\omega$ reaction and decays of generated ω meson are also measured with $\omega \rightarrow \pi^0\gamma$ mode. Such exclusive measurement can supply essential information to establish partial restoration of the chiral symmetry in nucleus.

References

- [1] T. Hatsuda and S.H. Lee, Phys. Rev. **C46** (1992) R34.
- [2] T. Hatsuda and T. Kunihiro, Phys. Rep. **247** (1994) 221.
G.E. Brown and M. Rho, Phys. Rep. **269** (1996) 333.
W. Cassing and E.L. Bratkovskaya, Phys. Rep. **308** (1999) 65.
- [3] K. Suzuki *et al.* , Phys. Rev. Lett **92** (2004) 072302.
- [4] K. Ozawa *et al.* , Phys. Rev. Lett **86** (2001) 5019.
M. Naruki *et al.* , Phys. Rev. Lett **96** (2006) 092301.
R. Muto *et al.* , Phys. Rev. Lett **98** (2007) 042501.
- [5] M.A. Kagarlis *et al.* , Phys. Rev. **D60** (1999) 025203.
G.M. Huber *et al.* , Phys. Rev. **C68** (2003) 065202.
- [6] D. Trnka *et al.* , Phys. Rev. Lett. **94** (2005) 192303.
- [7] C. Djalali *et al.* , J. Phys. **G34** (2007) S495.
- [8] F. Klingl, N. Kaiser and W. Weise, Nucl. Phys. **A624** (1997) 527.
F. Klingl, N. Waas and W. Weise, Nucl. Phys. **A650** (1999) 299.
- [9] M.F.M. Lutz, Gy. Wolf and B. Friman, Nucl. Phys. **A706** (2002) 431.
- [10] P. Muehlich *et al.* , Nucl. Phys. **A780** (2006) 187.
- [11] H. Kurasawa and T. Suzuki, Prog. Theor. Phys. **84** (1990) 1030.
H. C. Jean, J. Piekarewicz and A. G. Williams, Phys. Rev. **C49** (1994) 1981.
K. Saito, K. Tsushima, A. W. Thomas and A. G. Williams, Phys. Lett. **B433** (1998) 243.
K. Tsushima, D. H. Lu, A. W. Thomas and K. Saito, Phys. Lett. **B443** (1998) 26.
B. Friman, Acta Phys. Polon. **B29** (1998) 3195.
M. Post and U. Mosel, Nucl. Phys. **A688** (2001) 808.
K. Saito, K. Tsushima, D. H. Lu and A. W. Thomas, Phys. Rev. **C59** (1999) 1203.
G. I. Lykasov, W. Cassing, A. Sibirtsev and M. V. Rzyanin, Eur. Phys. J. **A6** (1999) 71.
A. Sibirtsev, C. Elster and J. Speth, nucl-th/0203044.
A. K. Dutt-Mazumder, R. Hofmann and M. Pospelov, Phys. Rev. **C63** (2001) 015204.

- M. F. M. Lutz, G. Wolf and B. Friman, Nucl. Phys. **A706** (2002) 431 [Erratum-ibid. **A765** (2006) 431].
 S. Zschocke, O. P. Pavlenko and B. Kampfer, Phys. Lett. **B562** (2003) 57.
 A. K. Dutt-Mazumder, Nucl. Phys. **A713** (2003) 119.
 P. Muehlich, T. Falter and U. Mosel, Eur. Phys. J. **A20** (2004) 499.
 P. Muehlich, V. Shklyar, S. Leupold, U. Mosel and M. Post, nucl-th/0607061.
 P. Muehlich and U. Mosel, Nucl. Phys. **A773** (2006) 156.
 B. Steinmueller and S. Leupold, hep-ph/0604054
- [12] E. Marco and W. Weise, Phys. Lett **B502** (2001) 59.
- [13] H. Nagahiro, D. Jido, and S. Hirenzaki, Nucl. Phys. **A761** (2005) 92.
 H. Nagahiro, D. Jido, S. Hirenzaki, e-Print: arXiv:0811.4516 [nucl-th]. H. Nagahiro, private communication.
- [14] M. Kaskulov *et al.* , Phys. Rev. **C75** (2007) 064616.
- [15] R.E. Chrien *et al.* , Phys. Rev. Lett. **60** (1988) 2595.
- [16] "The FLUKA code: Description and benchmarking" G. Battistoni, S. Muraro, P.R. Sala, F. Cerutti, A. Ferrari, S. Roesler, A. Fasso', J. Ranft, Proceedings of the Hadronic Shower Simulation Workshop 2006, Fermilab 6-8 September 2006, M. Albrow, R. Raja eds., AIP Conference Proceeding 896, 31-49, (2007)
- "FLUKA: a multi-particle transport code" A. Fasso', A. Ferrari, J. Ranft, and P.R. Sala, CERN-2005-10 (2005), INFN/TC_05/11, SLAC-R-773
<http://www.fluka.org/fluka.php>
- [17] D.V. Dementyev *et al.* , Nucl. Instrum. Meth. **A440** (2000) 151.
- [18] G. Penner and U. Mosel, Phys. Rev. **C65** (2002) 055202.
- [19] J. E. Nelson *et al.* , Phys. Lett **B47** (1973) 281.
- [20] S. Prakhov *et al.* , Phys. Rev. **C69** (2004) 045202.
- [21] J. Keyne *et al.* , Phys. Rev. **D14** (1976) 28.
- [22] J.G. Messchendorp, A. Sibirtsev, W. Cassing, V. Metag, and S. Schandmand, Eur. Phys. J. **A11**, 95-103 (2001))